Study of beach permeability's influence on solitary wave runup with ISPH method

Chiaki Tsurudome[1, 2], Dongfang Liang[1*], Yuma Shimizu[3], Abbas Khayyer[3], Hitoshi Gotoh[3]

[1]Department of Engineering, University of Cambridge, Cambridge CB2 1PZ, UK

[2]Civil Engineering Research Laboratory, Central Research Institute of Electric Power Industry, Abiko, Chiba 270-1194, Japan

[3]Graduate School of Engineering, Kyoto University, Nishikyo-ku, Kyoto 615-8450, Japan

* corresponding author

Abstract Coastal protections, such as dykes, seawalls, breakwaters and natural beaches can often be considered as porous structures. The accurate prediction of wave motion around porous structures is necessary for the effective design of durable coastal protections. Smoothed particle hydrodynamics (SPH) is a meshless particle-based method suitable for the simulations of violent free-surface flows and their interaction with structures. In this paper, an incompressible SPH (ISPH) model is applied to the simulations of solitary wave runup on permeable slopes. The apparent density concept is introduced to allow the smooth particles' volume to change when shifting between the pure-fluid region and porous region. The present simulations consider both the triangular beaches with uniform permeability and the solid beaches with overlying porous layers. The study focuses on the influence of permeability on the maximum wave runup heights. New runup laws are proposed, which offer guidelines for the design of porous coastal protections.

Keywords: SPH; ISPH; solitary wave; runup; porous structure; permeability

1. Introduction

Wave runup height is a critical factor for designing coastal structures, such as revetments, breakwaters and seawalls. These structures are often constructed to mitigate the risk of wave attacks, including storm surges and tsunami waves. As the wavelength of tsunamis is long, its phase speed is proportional to the square root of the water depth.

In shallow waters, the height of a tsunami grows, while the propagation speed decreases. Tsunami waves moving in shallow waters can break and cause severe damage on coastal structures (Lo and Shao, 2002). Among the most catastrophic events in recent history is the Sumatra Tsunami on 26 December 2004. Induced by an underwater earthquake, this tsunami hit Indonesia, Thailand, Malaysia, Myanmar, Bangladesh, India, Sri Lanka, Maldives and coastal countries in Africa; the number of dead and missing was over 226,000. Similarly, a 9.0 MW earthquake occurred off the Pacific coast of Tohoku, Japan, on 11 March 2011. The resulting tsunami inundated over 400 km^2 of land, leaving more than 20,000 people dead or missing. These mega disasters highlight the importance of effective management of coastal areas.

Tsunami waves have traditionally been conveniently modelled as solitary waves (Lin et al., 1999; Chang et al., 2009, Liang et al. 2013b). Large-scale experiments of solitary wave runup on idealised slopes have been conducted to investigate the tsunami wave interaction with beaches. Hall and Watts's (1953) experiment is among the earliest studies of solitary wave runup on a plane slope. Later, Synolakis (1986) conducted a series of classical experiments on solitary wave propagation over a 1:19.85 sloped beach. In his study, wave profiles were captured and compared with the analytical solutions. Chang et al. (2009) conducted similar experiments to re-examine the behaviour of breaking waves with improved and detailed measurement on a 1:20 slope. As for very mild beaches, Hsiao et al. (2008) conducted large-scale experiments of wave runup on a 1:60 slope.

Various numerical models have been applied to the study of the interaction between solitary waves and coastlines. Lin et al. (1999) investigated solitary wave runup and rundown on a 1:20 slope using a Reynolds-Averaged Navier–Stokes (RANS) model. They analysed the pressure and velocity fields during the runup and rundown processes.

The wave profiles were compared with those obtained in experiments, the solutions to the Boussinesq equations and the results of the shallow water equations. Xiao and Huang (2008) also utilised a RANS model, with the *k*-ε turbulence closure, to investigate solitary wave runup on a 1:20 slope. Liang et al. (2013a, 2013b) coupled the Boussinesq and non-linear shallow-water equations to investigate solitary wave and N-wave interactions with uniform slopes. Owing to its capability of capturing violent free-surface deformations, Smoothed Particle Hydrodynamics (SPH) has also been applied to solitary wave runup problems. Monaghan and Kos (1999), for instance, studied the wave impact on typical Cretan beach using a numerical wave flume based on the weakly compressible SPH (WCSPH) method. Meanwhile, Kim and Ko (2008) and Memarzadeh and Hejazi (2012) investigated the solitary wave runup on a relatively steep slope with the incompressible SPH (ISPH) method. The ISPH model was also used by Shadloo et al. (2015) to study the wave dynamics on a mild slope.

Almost all the above-mentioned studies assume a solid impermeable slope as a representation of the natural beach. Actual beaches generally consist of sand, pebbles, cobbles, gravels or vegetations. Shao (2010) presented an innovative investigation to apply the ISPH method to flows through porous media. In his model, the effect of the porous media on the flow is described by an additional friction force. An imaginary grid line is defined at the interface between the porous region and the fluid region. Ren et al. (2016) implemented a WCSPH framework to simulate wave motion and turbulent flow around porous media. They set the background porosity points which contained porosity information and proposed a transition zone between fluid and porous regions. The gradual transition of porosity helped avoid numerical instabilities. Many efforts have been made to improve porous flow modelling in the last decade (Pahar and Dhar, 2017; Khayyer et

al. 2018; Kazemi et al. 2020a; Kazemi et al. 2020b; Wen et al. 2020). Qu et al. (2019) applied a nonhydrostatic model to the simulations of wave runup through gravel layers overlaying an impermeable slope. Tsurudome et al. (2020) simulated solitary wave propagation over a permeable beach using the ISPH method, which contained only limited steep slope cases. Lucy et al. (2021) investigated the solitary wave interactions with sandy seawalls and uniformly sloped beaches with a Material Point Method (MPM), which is another type of meshfree method.

For sandy beaches or beaches covered with thick vegetation layers, they do not behave as solid boundaries and their permeability has to be considered in order to accurately estimate the runup heights. In this paper, an ISPH model is established to simulate the solitary wave runup on permeable slopes of different gradients. Firstly, wave runup on a solid slope is briefly reviewed and verified. Then, permeable triangular beaches are considered in both steep and mild slopes. Finally, the situation of a permeable layer overlying a solid beach is considered. The empirical relationship between the runup height and beach permeability is established.

2. ISPH model for flows inside and outside porous media

2.1 Governing equations

The governing equations are the momentum-conservation equation and mass-conservation equation. Ren et al. (2016) derived the precise equations governing the porous flow, which have also been used in Akbari and Toarbbeigi (2021), Kazemi et al. (2020) and Wen et al. (2020). The current study adopts a simplified version of those equations by disregarding the spatial and temporal variations of the porosity. Because the porous media are immobile in this study, the time derivative of the porosity is indeed zero.

The spatial derivative of the porosity is non-zero only at the boundary of the porous media, i.e., the interface between the pure liquid region and porous region. Since all numerical simulations need to introduce an artificial transition layer between the pure-liquid region and the porous region to maintain numerical stability, the spatial variation of the porosity is numerical rather than physical. As a result, the accurate evaluation of the spatial derivative of the porosity is not crucial for the present study.

$$\frac{D\boldsymbol{u}}{Dt} = -\frac{1}{\rho}\nabla P + \boldsymbol{g} + \nu\nabla^2\boldsymbol{u} + \frac{1}{\rho}\nabla\cdot\boldsymbol{\tau} + \frac{\boldsymbol{R}}{\rho}\ , \tag{1}$$

$$\frac{1}{\rho}\frac{D\rho}{Dt} + \nabla\cdot\boldsymbol{u} = 0, \tag{2}$$

where $\frac{D}{Dt}$ represents the material derivative, $\boldsymbol{u}$ is the liquid velocity, ρ is the density, P is pressure, $\boldsymbol{g}$ represents the gravity acceleration vector, ν is the kinematic viscosity coefficient, $\boldsymbol{\tau}$ is the turbulent stress tensor that will be discussed later on, and $\boldsymbol{R}$ is the extra resistance force for the fluid flow inside the porous media that will be discussed in the next paragraph. In our model, the porous media are immobile and only the liquid movement inside and outside the porous media is computed. In the pure liquid region, the definitions of the velocity and density are apparent. Inside the porous media, the velocity in Equations (1-2) should be understood as the actual pore liquid velocity or the intrinsic velocity, which is equal to the Darcy velocity divided by porosity, while the density should be taken to be the apparent density as detailed in the next section. When a liquid particle moves from the pure liquid region to the porous region, its mass does not change. However, its apparent density and volume shall increase to take into account that liquid can only occupy the intergranular pores. Consequently, liquid particles move in the porous region according to the intrinsic velocity.

Inside the porous media, the effect of the solid skeleton on the fluid flow can be modelled by an additional resistance force $\boldsymbol{R}$, whose value can be calculated with Ergun's law (Peng et al., 2017; Khayyer et al., 2018).

$$\boldsymbol{R} = -\frac{\mu}{Kp}\boldsymbol{u} - \frac{1.75}{\sqrt{150}}\frac{\rho}{\sqrt{Kp}Nw^{\frac{3}{2}}}|\boldsymbol{u}|\boldsymbol{u} \tag{3}$$

where μ is the dynamic viscosity coefficient, Kp is the intrinsic permeability, and Nw is the porosity. For flow inside a porous structure, $\boldsymbol{R}$ calculated by Equation (3) represents the drag force imposed on the liquid by the solid skeleton of the porous media. For flow outside the porous medium, $\boldsymbol{R}$ is set to zero and thus this extra resistance force vanishes from the momentum equation.

It should be noted that the porous media may be considered to be made of sediment, such as sandy beaches and rubble mound breakwaters, vegetation layer, such as coastal forests and mangrove swamps, or engineering materials, such as permeable bricks and pavements. This study focuses on the isolated influence of permeability on the wave runup, while porosity is fixed and the surface of the porous media is assumed to be smooth. We are currently undertaking studies on the influences of porosity and surface roughness of porous media and will report the findings in another paper.

2.2 ISPH algorithm

The detailed explanation of the ISPH algorithm can be found in Lo and Shao (2002), Shao and Lo (2003) and Khayyer et al. (2009, 2018). The pressure is obtained by the solution of the Pressure Poisson Equation (PPE). In this study, the source term for the PPE is a combination of the standard source term and the higher-order source (HS) term. The HS scheme was first developed by Khayyer et al. (2009). The modified PPE thus becomes:

$$\nabla \cdot \left(\frac{1}{\rho_*}\nabla P_{t+1}\right)_i = \gamma \frac{1}{\rho_0 \Delta t}\left(\sum_j m_j \nabla_i W_{ij} \cdot \boldsymbol{u}_{ij}\right)_i^* + (1-\gamma)\frac{\rho_0 - \rho_*}{\rho_0 \Delta t^2}, \quad (4)$$

where γ is the combination ratio, m_j is the mass of the smooth particle j, W_{ij} is the value of the kernel function between particles i and j, $\nabla_i W_{ij}$ is the gradient of the kernel function with respect to the coordinates of particle i, $\boldsymbol{u}_{ij}$ represents $\boldsymbol{u}_j - \boldsymbol{u}_i$, *i.e.*, the velocity difference between particles i and j, Δt is time step, the subscript t+1 represents quantity at the next time level, the subscript 0 denotes the initially specified reference values, and * denotes the quantities at the intermediate stage. The computational results are sensitive to the value of the combination ratio γ. The present numerical experiments show that γ = 0.97 leads to the best results, which is consistent with the findings by Gui et al. (2015). In this study, a C2 Wendland kernel (Wendland, 1995) is adopted. The complete implementation of the ISPH algorithm can be found in Liang et al. (2017) and Tsurudome (2020).

2.3 Apparent density

As the fluid particles can only occupy the void in the solid skeleton, the apparent density concept (Akbari, 2014) is adopted to modify the fluid particle density in the porous region of the computational domain. The apparent density and volume of a fluid particle at location i are defined as:

$$\rho_i = Nw_i \rho_w, \quad (5)$$

$$V_i = \frac{m_i}{\rho_i}, \quad (6)$$

where ρ_w is the density of the fluid in the region without porous media and Nw_i is the porosity at location i. Hence, if a fluid particle is located inside the porous media, the apparent density becomes less than ρ_w, which increases the apparent volume of the

particle. Therefore, particles are more sparsely distributed in the porous region than those in the pure fluid region. According to the smooth particle interpolation algorithm, a variable at position j can be approximated as:

$$\phi_j = \sum \phi_i W_{ij} \frac{m_i}{\rho_i} \tag{7}$$

where ϕ can be any variable, such as pressure or velocity, while the summation is over a compact neighbourhood where the kernel function is non-zero. It can be seen that the weight of the interpolation is increased in the porous medium region, as the fluid particles there have a smaller density and thus a larger volume. Hence, the sparser distribution of liquid particles in the porous region, as compared to the pure-fluid region, still satisfies the consistency condition.

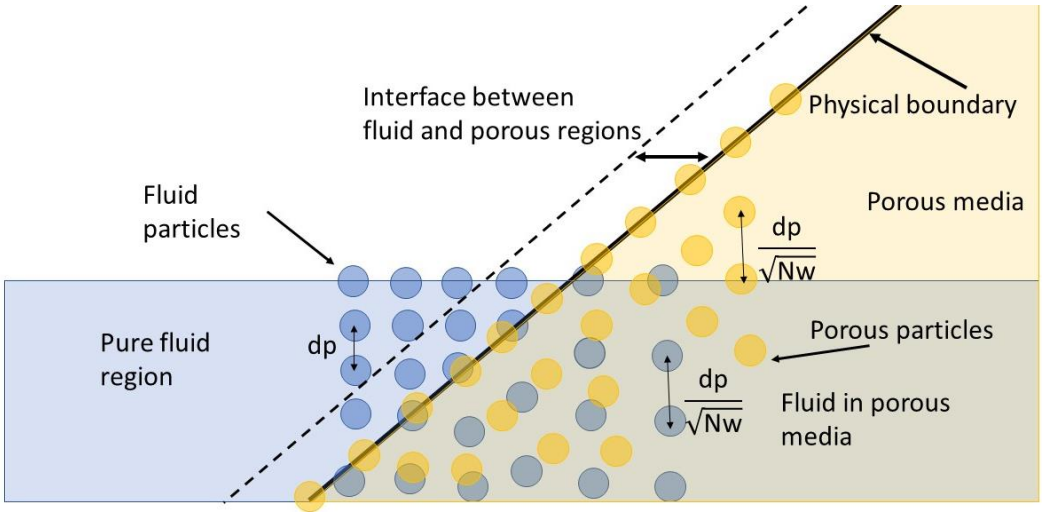

Figure 1 Schematic of the porous particle deployment

The porosity in the pure liquid region can be regarded to be one. In the current ISPH framework, the presence of the porous media is solely determined by existence of less-than-one porosity in the computational domain. The location of the porous media is prescribed by deploying dummy particles. Hereafter, these dummy particles are referred

to as porous particles. It should be noted that these porous particles are only used to indicate the location of the porous region and the calculation of the apparent densities at different positions. They are never involved in the ISPH computation. As seen in Figure 1, the fluid particles are initially configurated with spacing *dp* in the pure liquid region and with spacing $\frac{dp}{\sqrt{Nw}}$ in the porous region. Immobile porous particles are placed at the outer boundary of and inside the porous media at spacing $\frac{dp}{\sqrt{Nw}}$. The smoothing length is fixed at $\frac{1.2dp}{\sqrt{Nw}}$ in the entire region, which ensures the consistent integral interpolation.

The apparent porosity at the position of a water particle *i*, Nw_i, is calculated according to the following equation.

$$Nw_i = 1 - (1 - Nw)\frac{\rho_{pi}}{\rho_p}, \tag{8}$$

where ρ_p is density of the porous material. ρ_{pi} denotes the density of porous media at the position of the water particle *i*, which can be evaluated to be:

$$\rho_{pi} = \sum_j m_{pj} W_{ij}, \tag{9}$$

where m_{pj} is the mass of the porous particle *j*. If no porous particles can be found in the neighbourhood centred at particle *i*, then the value of ρ_{pi} is set to zero.

The actual mass m_p and density ρ_p of porous particles are not important, since only the dimensionless porosity *Nwi* is used in the ISPH solution of the governing equations. In the pure liquid region, the values of ρ_{pi} and Nw_i are 0 and 1, respectively, according to Equations (8-9), except in a thin layer adjacent to the boundary of the porous region. Similarly, in the porous region, the values of ρ_{pi} and Nw_i are ρ_p and *Nw*, respectively, except in a thin layer close to the porous boundary. As a liquid particle moves from the middle of the pure liquid region to the middle of the porous region, the

porosity associated with this particle changes from 1 to *Nw*. There is a transition layer centred at the interface between the pure liquid region and porous region, through which porosity gradually transits from 1 to *Nw*. The thickness of the transition layer is around two times the smoothing length, as indicated in Figure 1. Corresponding to the variation of porosity through this transition layer, the density of this liquid particle decreases from ρ_w to $Nw\rho_w$, and the volume of this liquid particle increases from m_i/ρ_w to $m_i/(Nw\rho_w)$.

2.4 Turbulence model

The Sub-Particle Scale (SPS) turbulence model (Gotoh et al., 2001, 2004) is coupled with the present ISPH method. In the SPS model, the additional turbulent stress tensor $\boldsymbol{\tau}$ is considered in the governing equation. The eddy viscosity assumption is adopted to express the turbulent stress tensor. After merging the turbulent kinetic energy term into the pressure term, the turbulent stress can be expressed as:

$$\frac{\boldsymbol{\tau}}{\rho} = 2\nu_t \boldsymbol{S} \tag{10}$$

where ν_t is the eddy viscosity coefficient. The SPS strain rate tensor $\boldsymbol{S}$ is:

$$\boldsymbol{S} = \frac{1}{2}(\nabla \boldsymbol{u} + \nabla \boldsymbol{u}^T) \tag{11}$$

The widely-used Smagorinsky model is adopted hereby to determine the turbulence eddy viscosity coefficient as follows:

$$\nu_t = (Cs\ dp)^2 |\boldsymbol{S}| \tag{12}$$

where *Cs* is the Smagorinsky constant set to 0.1 in this study, and *dp* is the initial particle spacing in the pure liquid region. The local strain rate magnitude $|\boldsymbol{S}|$ is defined by

$$|\boldsymbol{S}| = \sqrt{2\boldsymbol{S}:\boldsymbol{S}} \tag{13}$$

The developed model has been applied to a dam-break flow through a porous block and found to agree well with the experimental results of Liu et al. (1999). For further details about the numerical model and model verifications, readers are referred to Tsurudome et al. (2020).

2.5 Free surface particles

The particles located at the free surface need to be determined, whose pressure is set to zero before solving the Poisson pressure equation. Particle density has often been used to find free surface particles. If the density of particle *i* is smaller than a threshold value, then particle *i* is identified as a particle at the free surface. Traditionally, the particle density, associated with the free surface detection, is calculated by the following equation.

$$\rho_i^{Free-surface} = \sum_j m_j W_{ij} \tag{14}$$

However, in the porous region, the fluid particles are more sparsely distributed and the particle density defined in this way will always be smaller than the threshold value. Hence, the traditional way will lead to the false detection of free surface particles. In this study, Equation (14) is modified based on the porosity and apparent density of neighbouring fluid particles:

$$\rho_i^{Free-surface} = \sum_j \rho_j \left(\frac{dp}{\sqrt{N_{wj}}}\right)^2 W_{ij} \tag{15}$$

The reference density for particle *i* is calculated at each time step according to the instantaneous porosity and apparent density of particle *i*. In calculating the reference density for particle *i*, it is assumed that all the neighbouring fluid particles have the same

density as particle *i* and are regularly placed around the target particle *i* with spacing $\frac{dp}{\sqrt{Nw_j}}$, as shown in Figure 2.

$$\rho_i{}^{Reference} = \sum_j \rho_j \left(\frac{dp}{\sqrt{N_{wj}}}\right)^2 W_{ij}{}^{Reference} \tag{16}$$

$$W_{ij}{}^{Reference} = W\left(\left|\boldsymbol{r}_j{}^{Reference} - \boldsymbol{r}_i\right|, h\right)$$

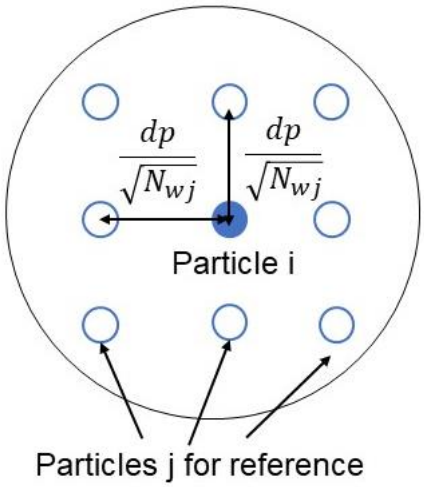

Figure 2 Virtual neighbouring particle distribution for calculating the reference density

The reference density calculated in this way basically assumes that the target particle *i* is an inner particle. The non-dimensional modified criterion is:

$$\frac{\rho_i^{Free-surface}}{\rho_i{}^{Reference}} < \theta \tag{17}$$

where the threshold ratio θ is a constant between 0.95 and 1.0. If this criterion is met, then particle *i* is regarded as a free surface particle. This method of judging the free surface particles is universally applicable to the porous region, pure fluid region and the transition region.

257

258

259 2.6 Wave-generation theory

260 A solitary wave is a single bulge of water above the still-water depth. Theories to
261 describe the wave profile have been proposed by Boussinesq. A solitary wave can be
262 generated in a wave flume by a piston (Goring, 1978). In this paper, such a piston-type
263 wavemaker is used to generate solitary waves in the simulation.

264 Based on the Rayleigh wave theory, Katell and Eric (2002) propose the following
265 equation for the paddle displacement:

$$X_R(t) = \frac{2\varepsilon}{\beta_R}\tanh\left[\frac{\beta_R(c_R t - X_R(t))}{2}\right], \quad \varepsilon = \frac{H}{h_0}\ , \tag{18}$$

266 where X_R is the horizontal position of the paddle, H is the initial wave height, h_0 is the
267 mean water depth, β_R is the outskirts decay coefficient and c_R is the wave speed given
268 by:

$$\begin{aligned} \beta_R &= \frac{1}{h_0}\sqrt{\frac{3\varepsilon}{1+\varepsilon}}, \\ c_R &= \sqrt{g(H+h_0)}. \end{aligned} \tag{19}$$

269 If the displacement of the paddle is small, then Equation (18) can be solved explicitly
270 after linearisation:

$$X_R(t) = \frac{2\varepsilon}{\beta_R}\frac{\tanh\left(\frac{\beta_R c_R t}{2}\right)}{1+\varepsilon\left[1-\tanh^2\left(\frac{\beta_R c_R t}{2}\right)\right]}. \tag{20}$$

271 The total stroke of the wave paddle will then simply become:

$$S_R = 4\sqrt{\frac{H(H+h_0)}{3}}. \tag{21}$$

272

3. Model verification: Wave runup on solid slopes

3.1 Wave runup laws

Many studies have been undertaken to predict wave runup height on solid beaches. Carrier and Greenspan (1953) obtained solutions of the non-linear shallow-water equations concerning the wave propagation over a slope. They presented findings of the nonbreaking waves during their climbing up a slope. Synolakis (1986) extensively investigated solitary wave runup height through experiments and analyses in his PhD thesis, with all key findings summarised in Synolakis (1987). He proposed the following law for nonbreaking waves:

$$\frac{R}{h_0} = 2.831(\cot\varphi)^{\frac{1}{2}}\left(\frac{H}{h_0}\right)^{\frac{5}{4}}, \tag{22}$$

and the following law for breaking waves on a 1:20 slope:

$$\frac{R}{h_0} = 1.109\left(\frac{H}{h_0}\right)^{0.582}. \tag{23}$$

In Equations (22) and (23), R is the maximum wave runup height, φ is a slope angle. R is defined as the maximum elevation that water reaches on the slope during runup, with the still water level coinciding zero elevation. Synolakis also found the critical wave heights beyond which waves would break on the slope, which were dependent on the slope angle.

$$\frac{H}{h_0} = 0.8183(\cot\varphi)^{-\frac{10}{9}}. \tag{24}$$

Since then, numerous improvements have been made to the above formulae. Li and Raichlen (2001) modified Synolakis's (1986) runup-height law for nonbreaking waves as follows.

$$\frac{R}{h_0} = 2.831(\cot\varphi)^{\frac{1}{2}}\left(\frac{H}{h_0}\right)^{\frac{5}{4}} + 0.293(\cot\varphi)^{\frac{3}{2}}\left(\frac{H}{h_0}\right)^{\frac{9}{4}}. \tag{25}$$

Equation (25) provides more accurate estimation of the runup heights, which agrees better with the experimental data in both relatively steep (1:2.08) and mild slopes (1:20). In estimating the runup height, Hughes (2004) first evaluated the nondimensional wave momentum flux M_F, using the first-order solitary wave theory:

$$\left(\frac{M_F}{\rho g h_0^2}\right)_{max} = \frac{1}{2}\left[\left(\frac{H}{h_0}\right)^2 + 2\left(\frac{H}{h_0}\right)\right] + \frac{N^2}{2M}\left(\frac{H}{h_0}+1\right)\left\{\tan\left[\frac{M}{2}\left(\frac{H}{h_0}+1\right)\right] + \frac{1}{3}\tan^3\left[\frac{M}{2}\left(\frac{H}{h_0}+1\right)\right]\right\}. \quad (26)$$

The coefficients M and N in Equation (26) can be approximated by the following empirical relationships:

$$M = 0.98\left\{\tanh\left[2.24\left(\frac{H}{h_0}\right)\right]\right\}^{0.44}$$
$$N = 0.69\tanh\left[2.38\left(\frac{H}{h_0}\right)\right]. \quad (27)$$

Hughes (2004) then derived the following runup law for nonbreaking solitary waves from the momentum flux:

$$\frac{R}{h_0} = 1.82(\cot\varphi)^{\frac{1}{5}}\left(\frac{M_F}{\rho g h_0^2}\right) \quad (28)$$

Meanwhile, the following runup law for breaking solitary waves was obtained according to the momentum flux:

$$\frac{R}{h_0} = (1.39 - 0.027\cot\varphi)\left(\frac{M_F}{\rho g h_0^2}\right)^{\frac{1}{2}}. \quad (29)$$

3.2 A 1:2.08 slope

In this section, wave runup on a steep solid slope is examined. The setup of the computational domain is sketched in Figure 3. All of the walls and bottoms are solid. The

flat-bed section is 2.07 m long, which is followed by a plane beach with a 1:2.08 slope. The total horizontal length of the numerical wave flume is approximately 3.0 m. The water depth was set to 0.21 m. Solitary waves were generated at the left end, with different relative wave heights H/h_0 of 0.100, 0.163, 0.200, 0.250 and 0.300. Based on Equation (24), the wave height needs to be more than 1.8 times the water depth for the wave to break. Hence, all the considered waves are expected to be nonbreaking during the runup process. The essential parameters are listed in Table 1.

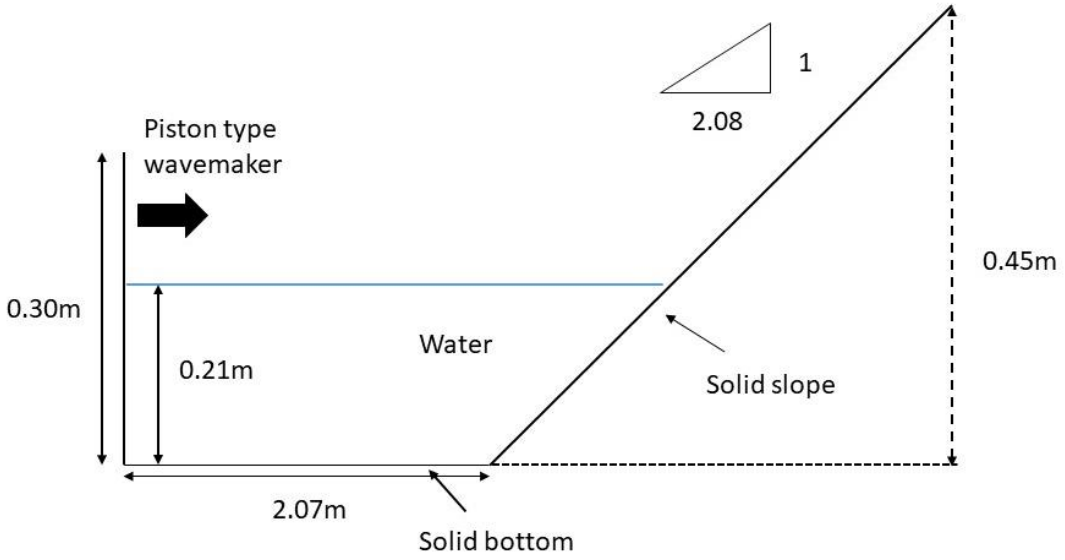

Figure 3. Setup of a 1:2.08 solid slope

Table 1. Computational parameters for wave runup on solid slopes

Parameters	Values
Diameter of particles (m)	0.005
Initial particle spacing (m)	0.005
Smoothing length (m)	0.006
Initial time step (s)	0.00025

Figure 4 compares the present ISPH simulation results with several past researches including the experimental measurements and the theoretical solutions. In our study, we

have checked that the wave height is kept nearly constant as the wave propagates over the flat-bed section, indicating insignificant numerical dissipation in the current simulations. As waves do not break on this steep slope, the mechanical energy of the system is expected to be conserved during the propagation and runup. Using the ISPH model, the computed relative runup height R/h_0 is predicted to be 0.469 with the wave H/h_0 = 0.163, and 0.848 with the wave H/h_0 = 0.25. Three runup-height theories show slightly different trends as H/h_0 increases. Li and Raichlen's (2001) law provides the closest match with the experimental results, whereas Synolakis's (1986) and Hughes' (2004) laws underestimate the runup height. The results of the present ISPH show good agreement with the theories and measurements for H/h_0 = 0.10 and 0.163. The relative difference between the present simulation and the experimental measurement is less than 7 % for these two cases. The present model tends to slightly overestimate runup height, as the incident wave height grows. However, the present results support the good performance of the Li and Raichlen's (2001) solution.

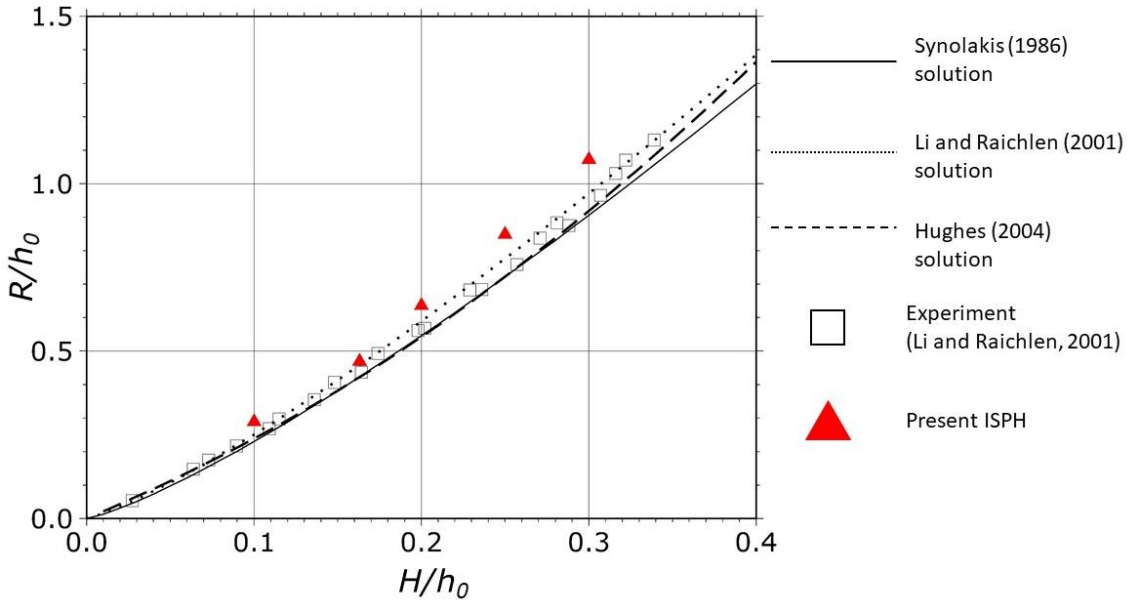

Figure 4. Runup heights on a 1:2.08 solid slope

3.3 A 1:20 slope

In this section, wave runup on a mild solid slope is investigated. The setup of the computational domain is illustrated in Figure 5. The flat-bottomed length is 2.00 m, followed by a 1:20 slope. The total horizontal length of the wave flume is approximately 10.0 m owning to the mild slope. The mean water depth is 0.21 m. A series of solitary waves are generated at the left end with the relative heights of H/h_0 = 0.100, 0.188, 0.280, or 0.416. From Equation (24), the threshold relative wave height is 0.0295, meaning that all the generated waves are expected to break when climbing up the slope. The simulation parameters are listed in Table 1.

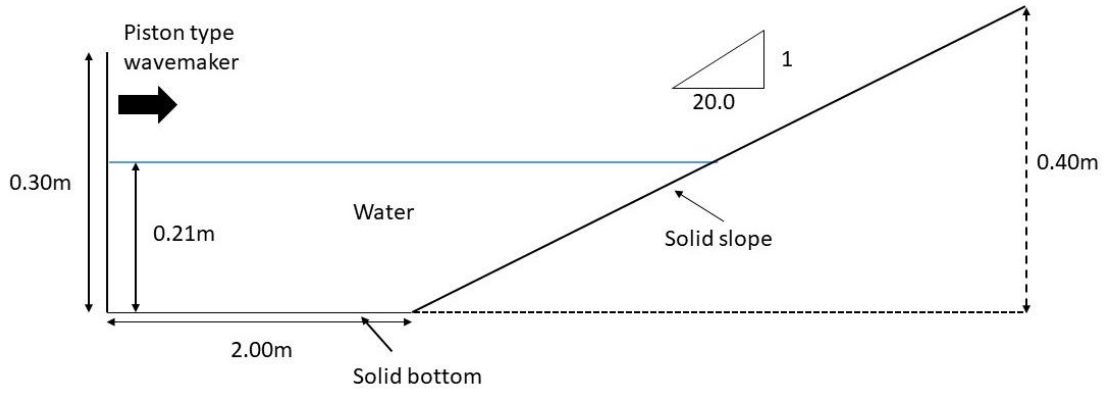

Figure 5. Setup of a 1:20 solid slope

Figure 6 compares the runup heights obtained from the present ISPH simulations, the experimental data, and the theoretical solutions. The relative difference between the ISPH simulations and the experimental data is around 14%, which is two times as large as the cases of nonbreaking waves. The runup heights simulated by the present ISPH tend to be lower than those observed in the experiments. However, the trend follows the

analytical solutions, and the ISPH results generally agree well with the runup-height law of Synolakis (1986).

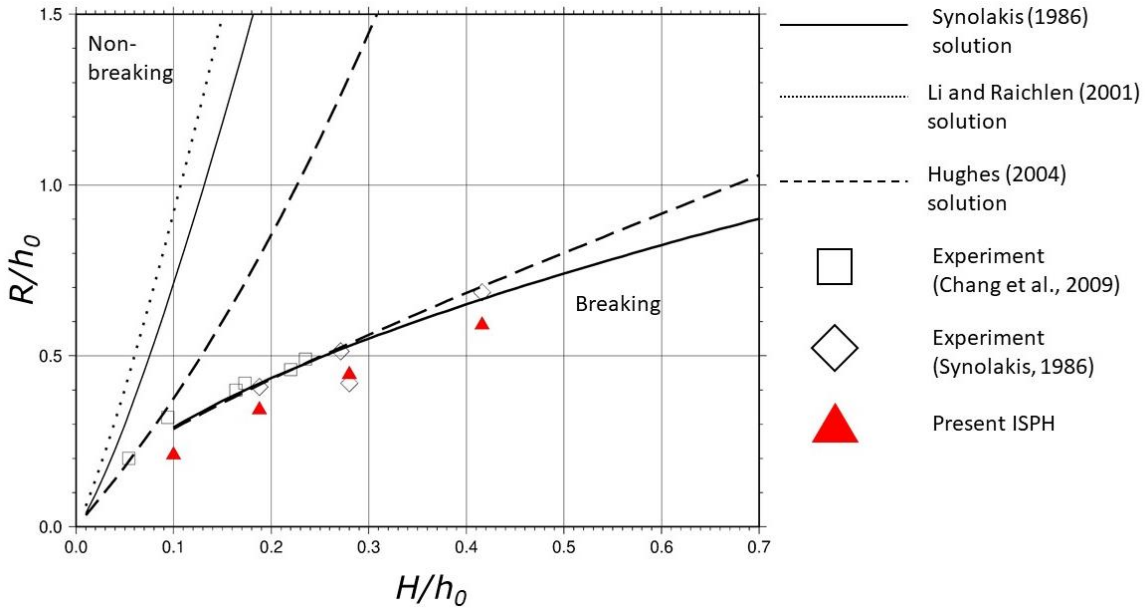

Figure 6. Runup heights on a 1:20 solid slope

4. Model Application 1: Permeable triangular beach

4.1 A 1:2.08 slope

In this section, wave runup on a mild permeable slope is simulated. The wave flume is 3.0 m long, and a triangle-shaped porous medium is located at x = 2.07 m − 3 m. The slope is 1:2.08 ($\varphi \approx 25.68°$). The dimensions of the domain are the same as those shown in Figure 3, but the slope is entirely permeable in this case. As seen in Equation (3), the interacting force between the porous beach structure and the moving water is affected by the beach permeability and porosity. In the following simulations, the permeability is varied, but the porosity of the slope is fixed at 0.49. The computational parameters are listed in Table 2. The mean water depth is 0.21 m, and two wave heights are tested: 0.03423 m (H/h_0 = 0.163) and 0.0525 m (H/h_0 = 0.25). In these simulations, the runup

height is defined as the highest point of the wave at the water-porous boundary. Although the same computational domain and settings were used in Tsurudome et al. (2020), further analysis and discussion on runup height are shown in this section.

Table 2. Computational parameters for wave runup on a 1:2.08 sloped porous beach

Parameters	Values
Diameter of particles (m)	0.005
Initial particle spacing of fluid particles (m)	0.005
Particle spacing of porous particles (m)	0.007
Smoothing length (m)	0.0085
Initial time step (s)	0.00025
Permeability of porous media (m^2)	1.21×10^{-10}, 1.88×10^{-10}, 7.54×10^{-10}, 3.02×10^{-9}, 1.21×10^{-9}, 3.02×10^{-7}, 1.21×10^{-6}, 7.54×10^{-6}, 3.02×10^{-5}, 1.21×10^{-4}

Figures 7 and 8 show typical snapshots of solitary wave runup on a permeable beach, with the permeability $Kp = 3.02 \times 10^{-7}\,m^2$ and $1.88 \times 10^{-10}\,m^2$, respectively. The initial wave height is 0.03423 m (H/h_0 = 0.163). When the permeability is $Kp = 3.02 \times 10^{-9} m^2$, the wavefront reaches the permeable slope at t = 3.50 s. The wave is partly blocked by the permeable beach as it is partially transmissive. At t = 4.05 s, the flow reaches the highest point on the permeable slope. Some fluid particles can be observed in the porous media located between the mean water level and the wave crest. These fluid particles penetrate through the permeable beach from the pure fluid region. In Figure 8, the wavefront appears to be chopped and discontinuous around the water-porous boundary due to low permeability. During runup, the water table keeps its initial level, at

0.21 m. Fluid particles slide on the permeable beach, and no particles penetrate through the water-porous boundary.

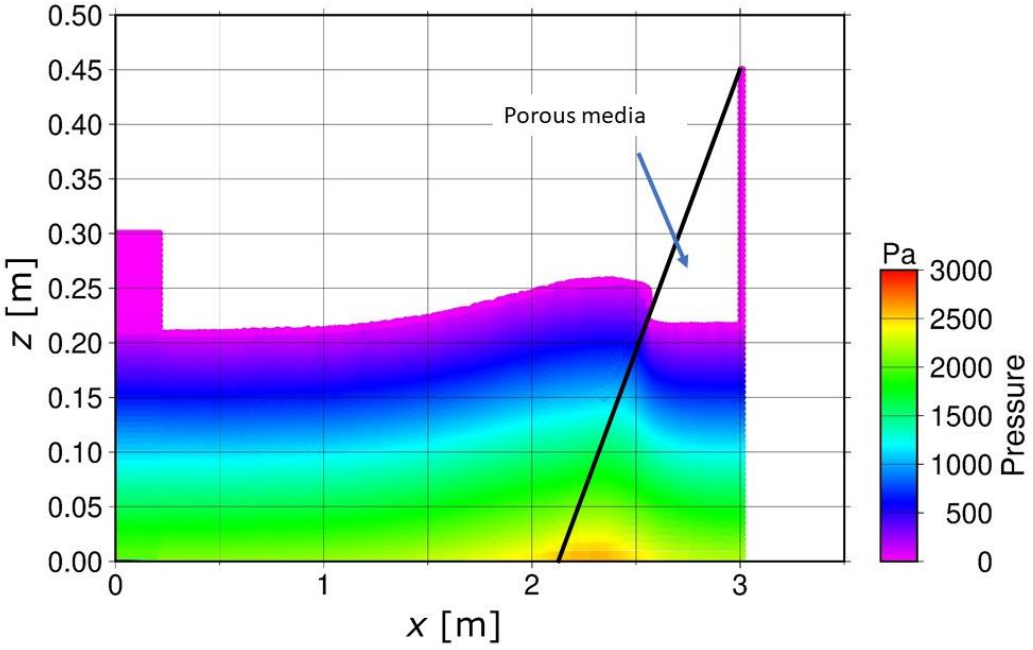

(a) t = 3.50 s

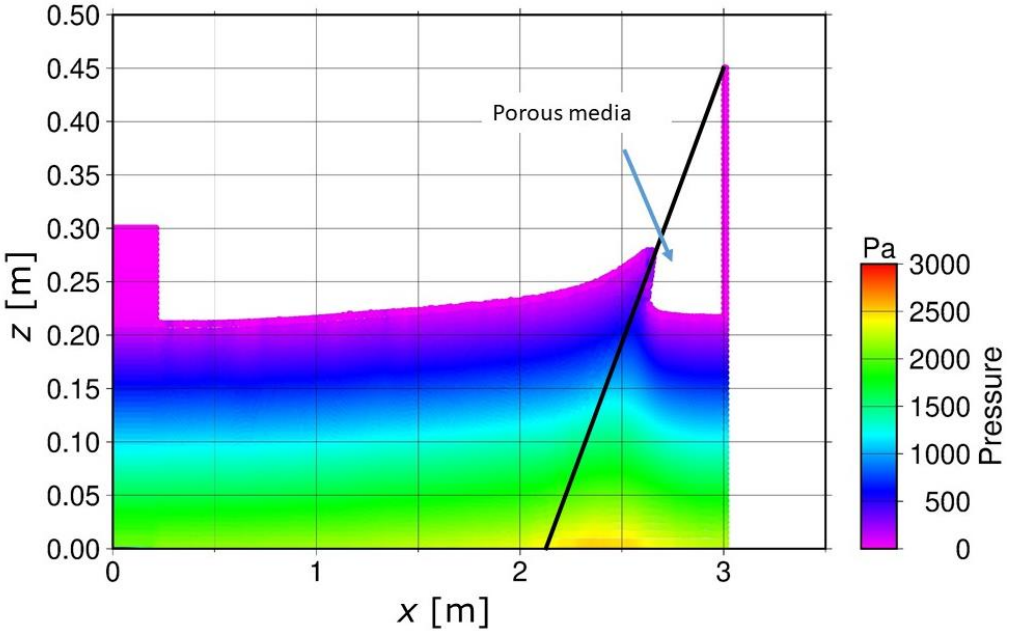

(b) t = 4.05 s

Figure 7. Wave propagation through a 1:2.08 sloped permeable beach ($Kp = 3.02 \times 10^{-9}\text{m}^2$)

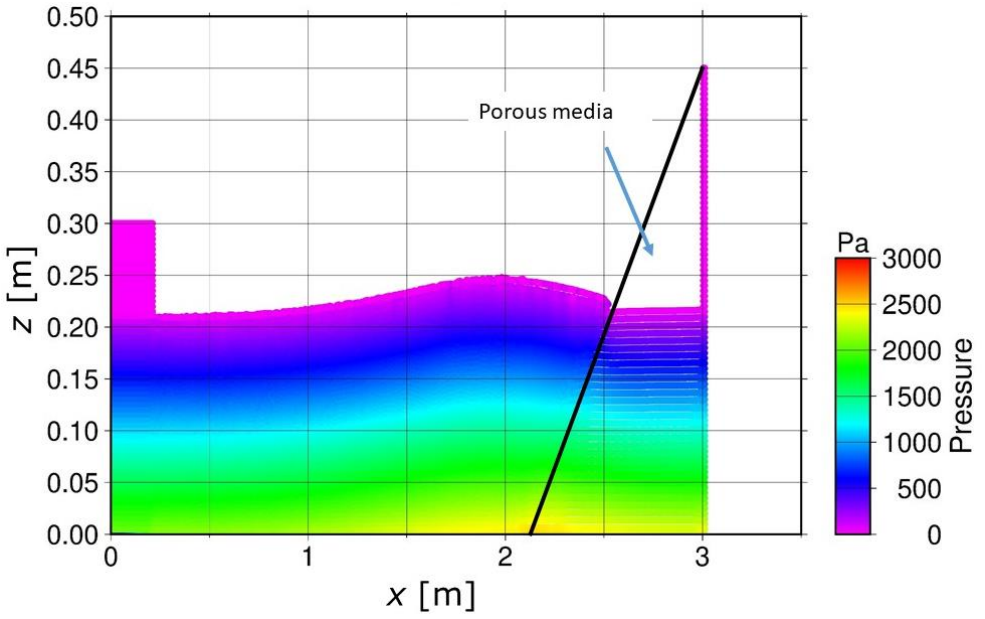

(a) t = 3.25 s

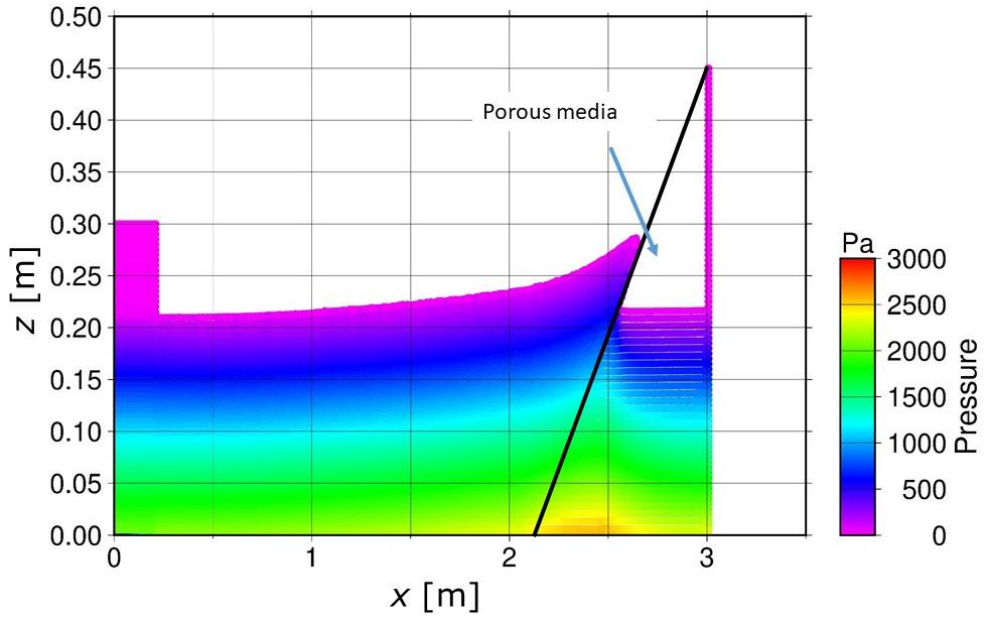

(b) t = 3.95 s

Figure 8. Wave propagation through a 1:2.08 sloped permeable beach (Kp =1.88 $\times 10^{-10}\text{m}^2$)

Figure 9 summarises the runup heights of the two different wave heights on beaches of various permeabilities. The horizontal axis is in logarithmic. The runup height decreases nearly linearly, as the permeability increases logarithmically. Therefore, there exists a power law between the runup height and the permeability.

Based on the data presented in Figure 9, the runup height law on permeable beaches can be expected to be:

$$R = k_1 K p^{k_2} \quad , \tag{30}$$

where k_1 and k_2 are coefficients. In our study, k_2 can be estimated at around −0.026 and k_1 can be estimated to be:

$$\begin{aligned} k_1 &= 44.7 \quad \text{for } H = 0.03423 \text{ m}, \\ k_1 &= 77.1 \quad \text{for } H = 0.0525 \text{ m}, \end{aligned} \tag{31}$$

In order to derive a universal formula, we assume that k_1 can be written as

$$k_1 = k_3 \frac{R_s}{(h_0^2)^{k_2}}, \tag{32}$$

where R_s is the runup height on the corresponding solid slope with the same incoming wave height H. Then, k_3 can be estimated to be 0.481 for both waves. The runup law for the wave propagating on a 1:2.08 permeable slope can be derived to be:

$$R = 0.481 R_s \left(\frac{Kp}{h_0^2}\right)^{-0.026} \quad . \tag{33}$$

In Figure 9, the dashed lines represent the estimated runup heights obtained through Equation (33) for two waves considered. With regard to the wave height of H = 0.03423 m, the estimated runup height agrees well with the simulated runup height for all grain diameters. Although Equation (33) tends to slightly overestimate height when the grain

size is relatively large for the wave height of H = 0.0525 m, the overall estimation is satisfactory. Hence, we can expect the equation (33) to describe a universal relationship for non-breaking waves.

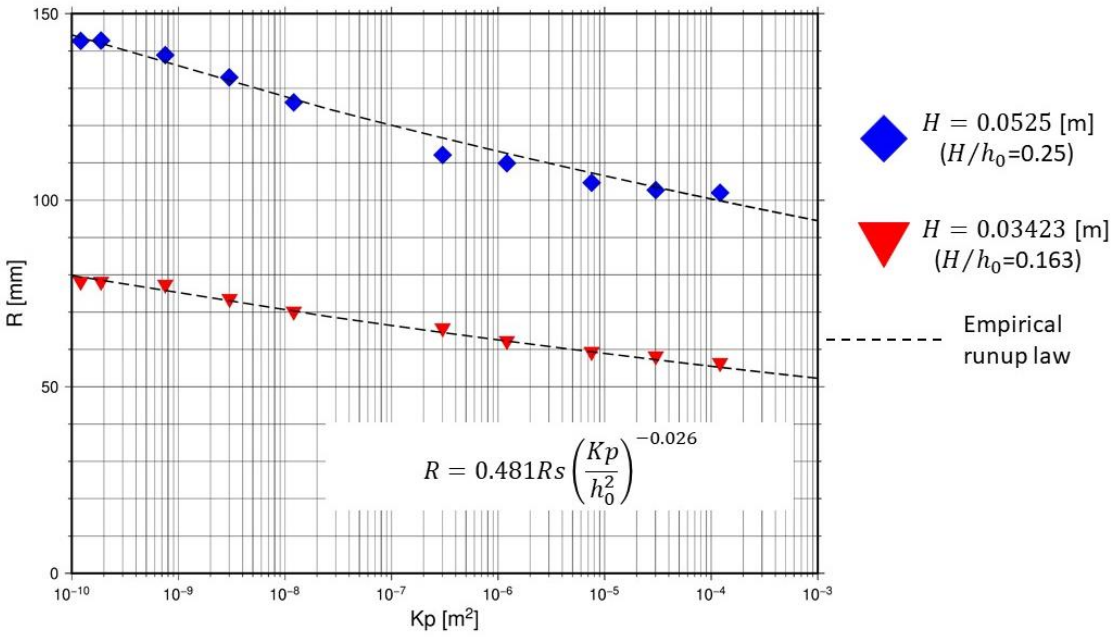

Figure 9. Empirical law for non-breaking wave runup height on a 1:2.08 sloped permeable beach

4.2 A 1:20 slope

The runup heights on a mild slope of various permeability are investigated in this section. A triangle-shaped porous medium is located at x = 2 m – 10 m, and the slope is now 1:20.0 ($\varphi \approx 2.86°$). The computational domain is the same as that shown in Figure 5, except that the slope material is porous in this case. The porosity of the porous media is fixed at 0.49, as in the previous section. The permeability varies from 1.21×10^{-10}m^2 to 1.21×10^{-4}m^2,. The computational parameters are listed in Table 2. The initial water depth was 0.21 m, and the generated wave height is 0.0588 m (H/h_0 = 0.28).

Figures 10 (a-b) and 11 plot the snapshots of solitary wave runup on permeable beaches with permeability of 3.02×10^{-9} m^2 and 1.88×10^{-10} m^2, respectively. Smooth and continuous pressure fields are obtained for both cases, thanks to the hybrid source term. At t = 6.00 s, the generated wave reaches the toe of the permeable beach and begins to run up. The shape of the wave becomes asymmetric at this instant. At t = 10.25 s, the wavefront reaches its highest point on the beach surface. While most of the fluid particles are blocked out of the porous medium, some particles can penetrate through the water-porous boundary when the permeability of the porous medium is 3.02×10^{-9}m^2. Conversely, if the permeability is 1.88×10^{-10}m^2, fewer particles can move from the pure fluid region into the porous area. Two example particle configurations are plotted in Figures 10(c-d), which show an enlarged part of Figures (a) and (b), respectively. The solid line represents the top porous boundary. Although the particle shifting technique (Lind et al., 2012; Khayyer et al., 2017) is not included in the present SPH model, particles are seen to be largely regularly distributed. The plots also highlight that the liquid particles are more sparse in the porous media, as part of the space is taken by the solid skeletons of the porous media.

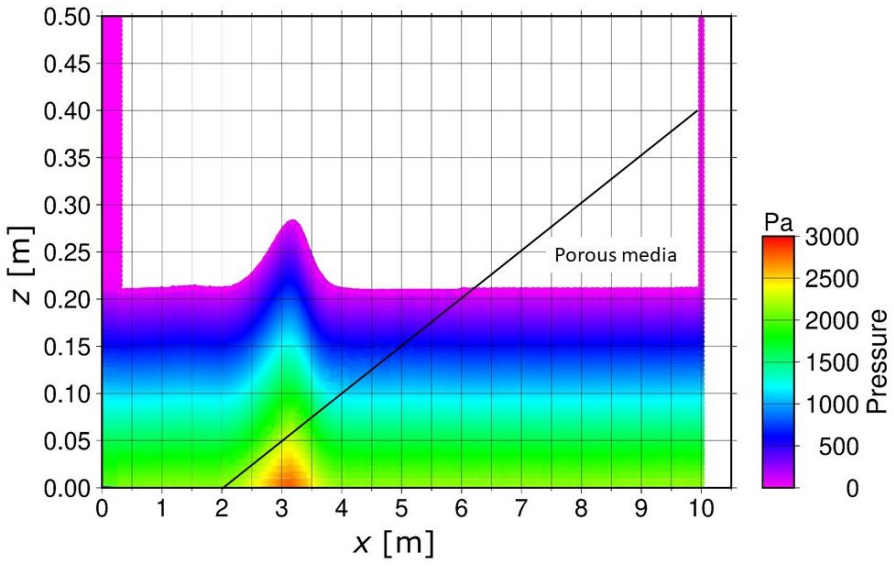

449 (a) t = 6.00 s

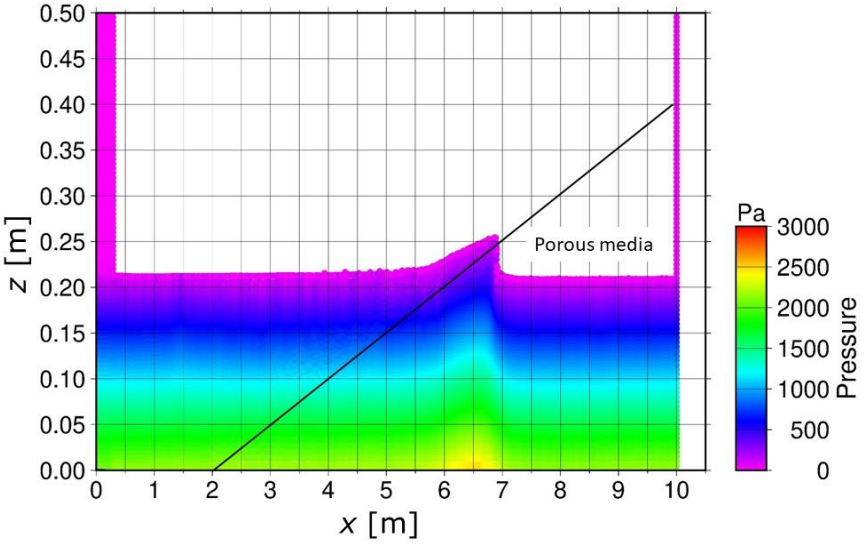

450

451 (b) t = 10.25 s

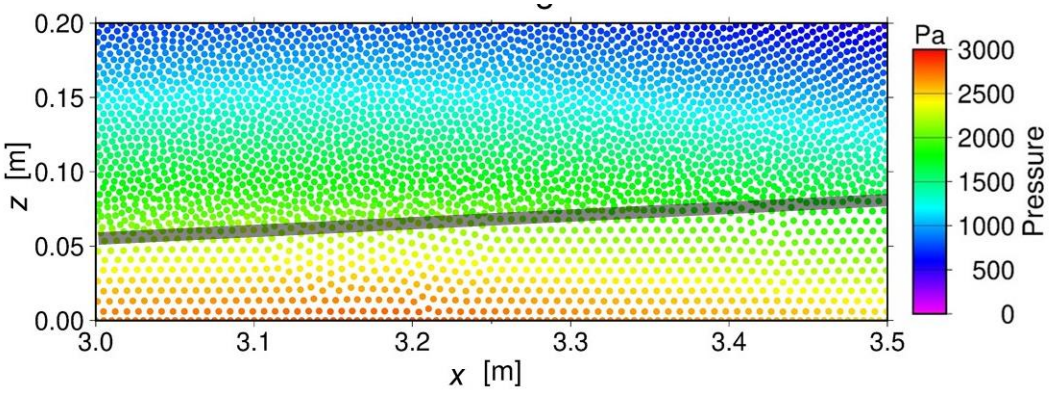

452

453 (c) A close-up of the particle configuration at t = 6.00 s

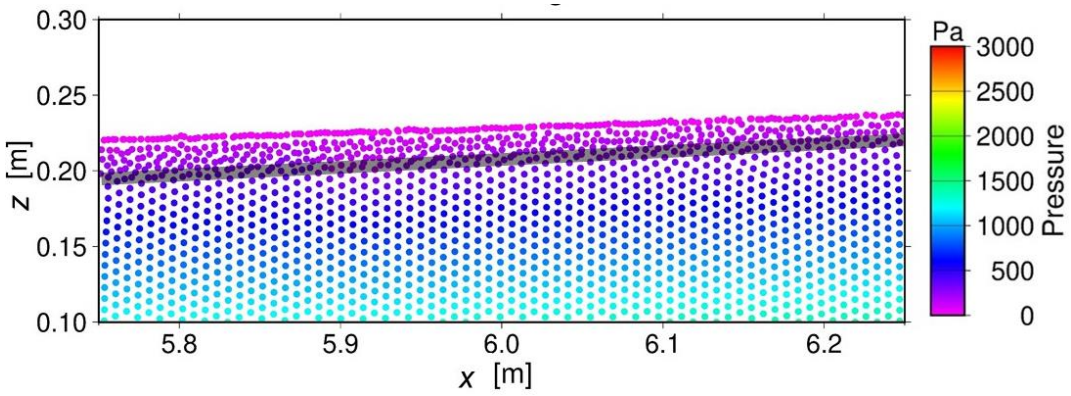

454

455 (d) A close-up of the particle configuration at t = 10.25 s

Figure 10. Wave propagation on a 1:20 permeable beach ($Kp = 3.02 \times 10^{-9}\text{m}^2$)

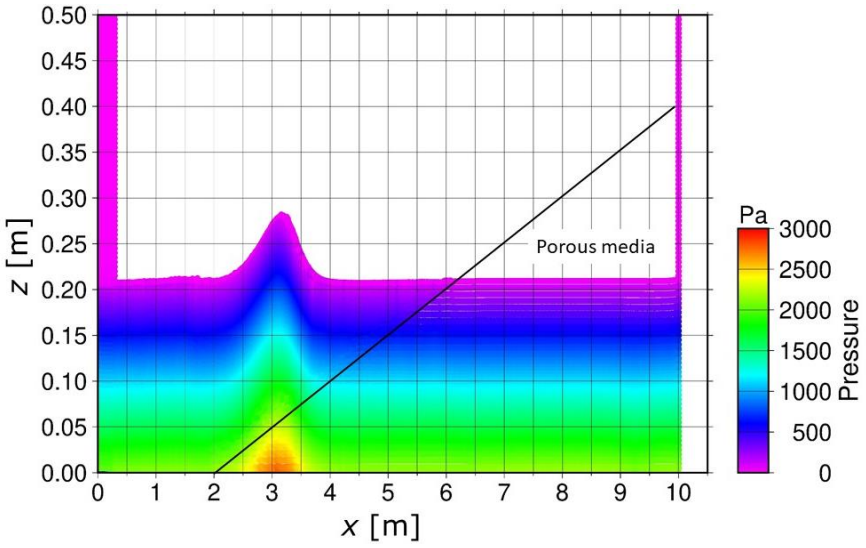

(a) t = 6.00 s

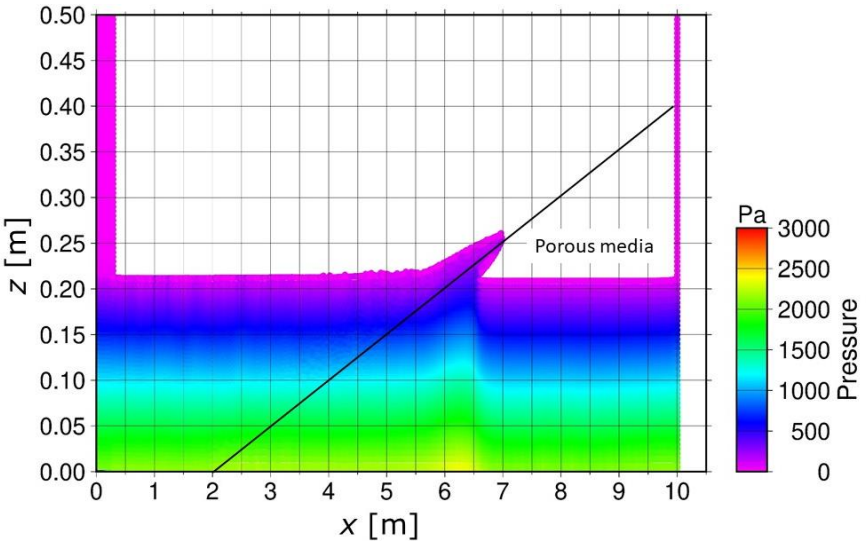

(b) t = 10.25 s

Figure 11. Wave propagation on a 1:20 permeable beach ($Kp = 1.88 \times 10^{-10}\text{m}^2$)

Figure 12 summarises the runup height for various permeability. Notably, the axes are in logarithmic scale. The runup height decreases nearly linearly as the permeability of the porous beach increases logarithmically. The decrease of runup height can be

significant. When $Kp = 1.88 \times 10^{-10}\,\mathrm{m}^2$, the runup height on the permeable slope decreases by 42% compared with the runup height on a solid slope.

Similar to the case of the steep slope, the runup height on this permeable beach can be expected to be:

$$R = k_1 R_s \left(\frac{Kp}{h_0^2}\right)^{k_2}, \tag{34}$$

where k_1 and k_2 are nondimensional coefficients. In our study, k_2 is around -0.059, whereas k_1 can be estimated to be around 0.164. The empirical runup law on this mild slope can be obtained as follows.

$$R = 0.164 Rs \left(\frac{Kp}{{h_0}^2}\right)^{-0.059} \tag{35}$$

In Figure 12, the dashed line represents the estimated runup height obtained through Equation (34) on a 1:20 permeable slope. The estimated runup height strongly agrees with the simulated runup height. As evidenced in the previous section, Equation (35) can be expected to be applicable to different wave heights and even slopes, as long as the incident wave breaks during runup. The term R_s is the runup height on the corresponding solid slope with the same wave height *H*. As a consequence, Equation (35) considers the effects of both the slope angle and wave height.

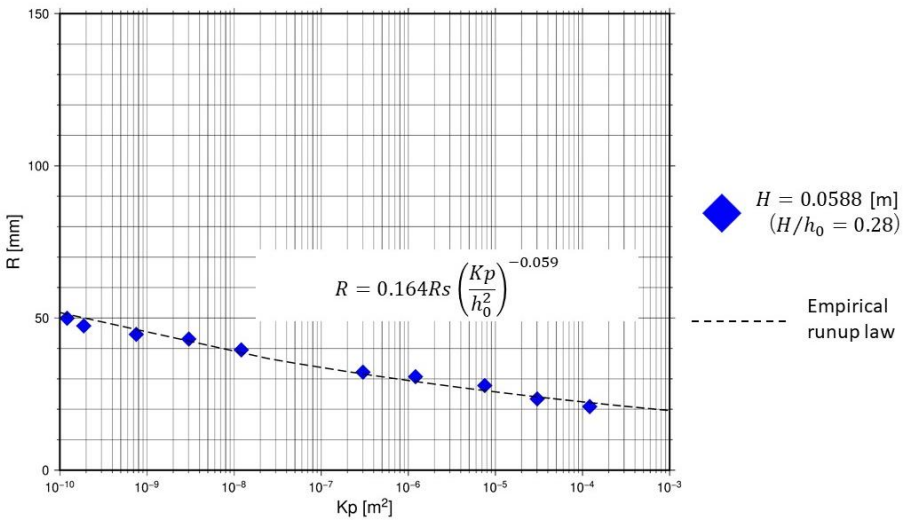

Figure 12. Empirical law for breaking solitary runup height on a 1:20 permeable beach

5. Model Application 2: Permeable layered beach

5.1 A 1:2.08 slope

This section considers a steep slope covered with different permeable layers. The schematic of the computational domain is presented in Figure 13. The parallelogram-shaped porous layer is placed with its bottom left corner at x = 2.07, and the beach slope is 1:2.08 ($\varphi \approx 25.68°$). The generated wave heights are H = 0.03423 m (H/h_0 = 0.163) or H = 0.0525 m (H/h_0 = 0.25) in different runs. The porosity of the porous layers is fixed at 0.49, while various values of permeability are tested. The thickness of the porous layer also varies from 13.0 cm, 19.5 cm, to 43.3 cm. The highest point of the flow on top of the porous layer is defined as the runup height. The numerical parameters are listed in Table 3.

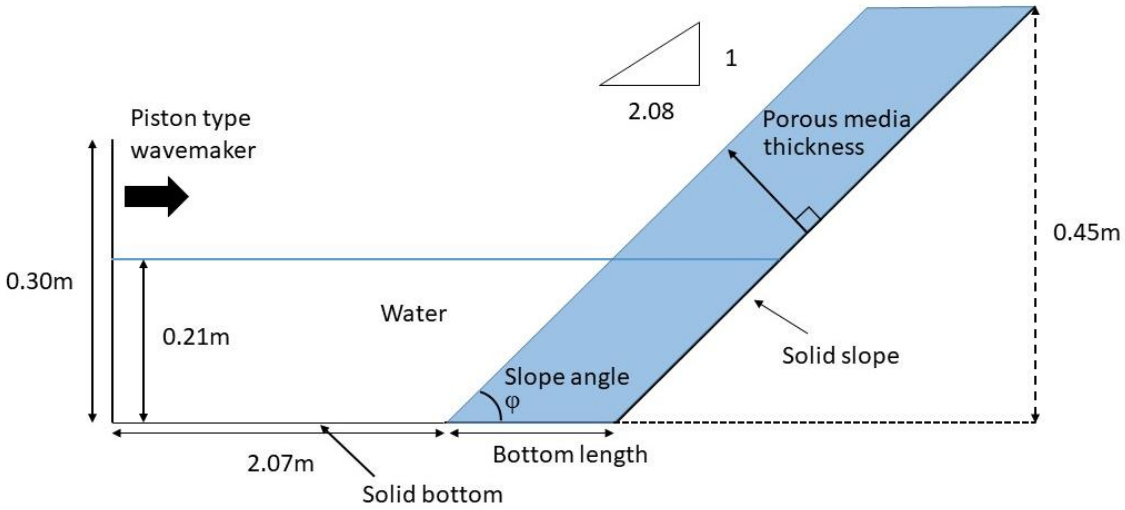

Figure 13. Setup of a 1:2.08 sloped porous layer

Table 3. Computational parameters for wave runup on 1:2.08 sloped porous layers

Parameters	Values
Diameter of particles (m)	0.005
Initial particle spacing of fluid particles (m)	0.005
Particle spacing of porous particles (m)	0.007
Smoothing length (m)	0.0085
Initial time step (s)	0.00025
Permeability of porous media (m^2)	1.21×10^{-10}, 1.88×10^{-10}, 7.54×10^{-10}, 3.02×10^{-9}, 1.21×10^{-9}, 3.02×10^{-7}, 1.21×10^{-6}, 2.71×10^{-6}, 4.82×10^{-6}, 7.54×10^{-6}, 3.02×10^{-5}, 1.21×10^{-4}
Bottom length of porous layers (cm)	30, 45, 100
Thickness of porous layers (cm)	13.0, 19.5, 43.3

Figure 14 shows the snapshots of the solitary wave runup on 13.0-cm-thick porous layers, with the permeability 3.02×10^{-9}m^2 and wave height H = 0.03423 m (H/h_0 = 0.163). The smooth pressure field is obtained over the entire domain, demonstrating good performance of the present ISPH model. While some fluid particles penetrate through the water-porous boundary at t = 3.92 s, most particles can only slide against the porous layer because of the different time scales of the movement inside and outside the porous layer.

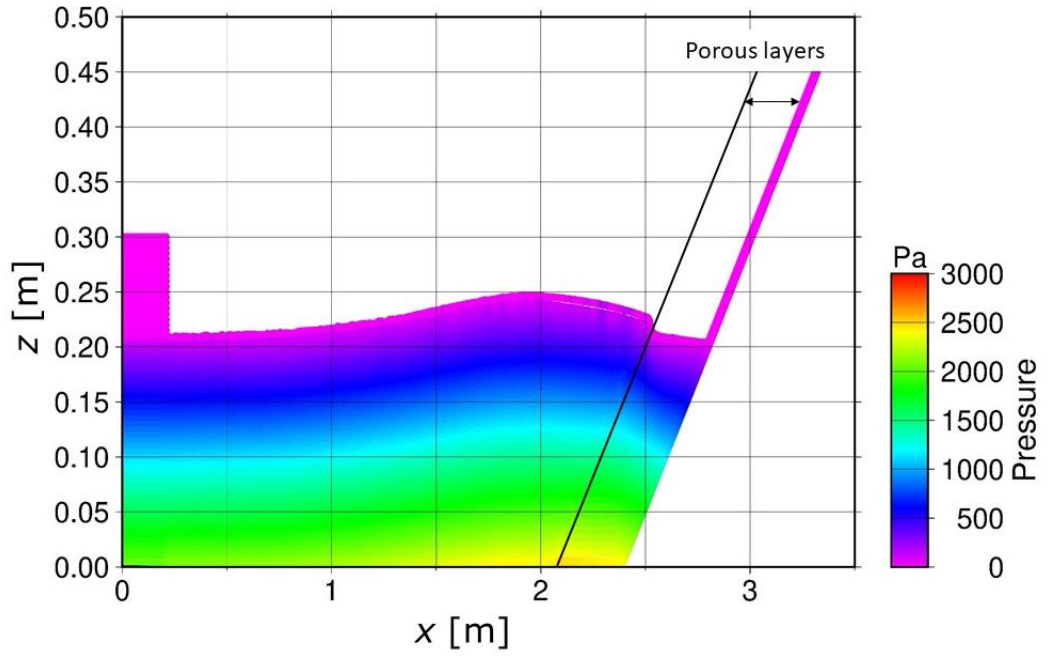

(a) t = 3.25 s

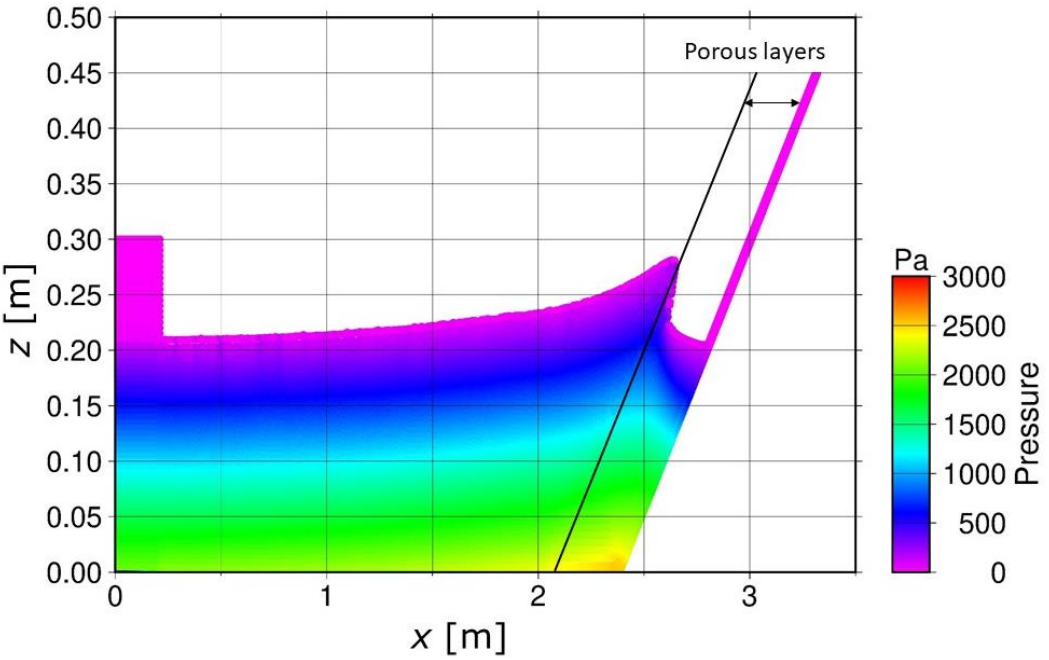

(b) t = 3.92 s

Figure 14. Wave runup on a 13.0-cm thick porous layer with Kp =3.02× 10^{-9}m^2 and H = 0.03423 m

When the incoming wave height is H = 0.03423 m (H/h_0 = 0.163), Figure 15 compares the runup height variations at three thickness values (13.0 cm, 19.5 cm, and 43.3 cm) and over a broad range of permeability values. The axes are in logarithmic scale. Overall, the runup height decreases nearly linearly as the permeability increases logarithmically. Almost the same height is obtained, regardless of the thickness of the porous media, until the permeability exceeds 2.71×10^{-6} m^2. When the permeability is greater than 4.82×10^{-6} m^2, the runup height on the 43.3-cm-thick layer becomes lower than those on thinner layers. There are only slight differences in the runup heights on layers of 13.0 cm and 19.5 cm in thickness, even when the permeability is larger than 4.82×10^{-6} m^2.

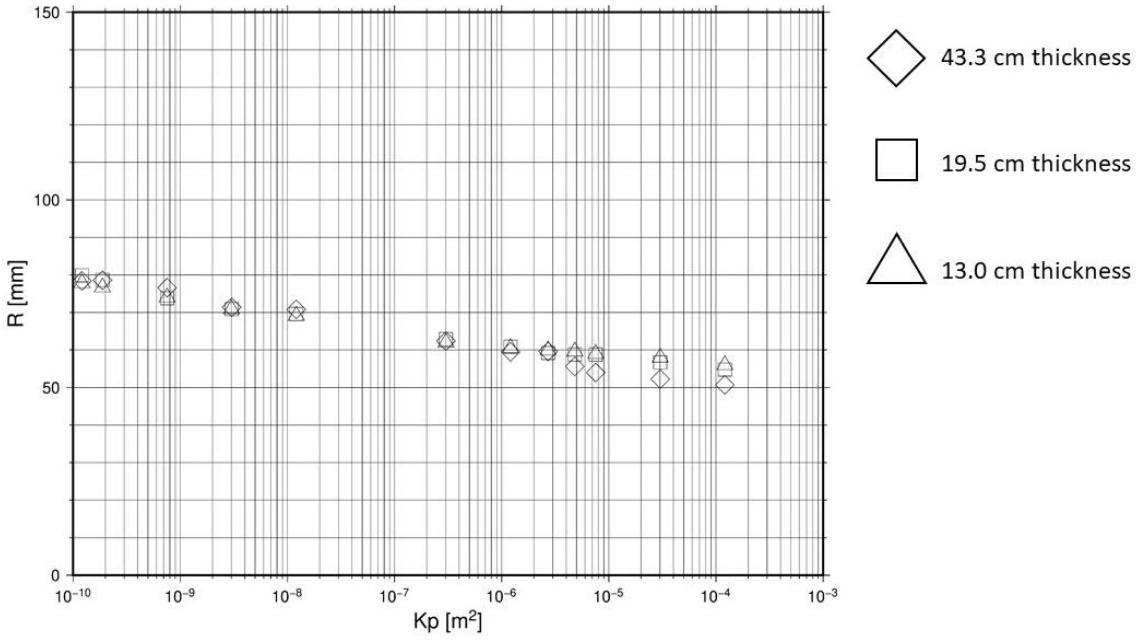

Figure 15. Runup height on 1:2.08 sloped porous layers with H = 0.03423 m

When the incoming wave height is increased to H = 0.0525 m (H/h_0 = 0.25), the results are summarised in Figure 16. The runup height decreases more rapidly with the increase of permeability, as compared to the case with a smaller wave height of H =

0.03423 m (H/h_0 = 0.163). The thickness of porous media does not affect the runup height until the permeability exceeds 3.02×10^{-7} m^2. If the permeability is 1.21×10^{-6} m^2 or larger, the 43.3-cm-thick layer yields lower runup than the other two thinner layers. The lower runup can be attributed to the fact that the fluid particles penetrate more deeply into the layer and spread out more widely.

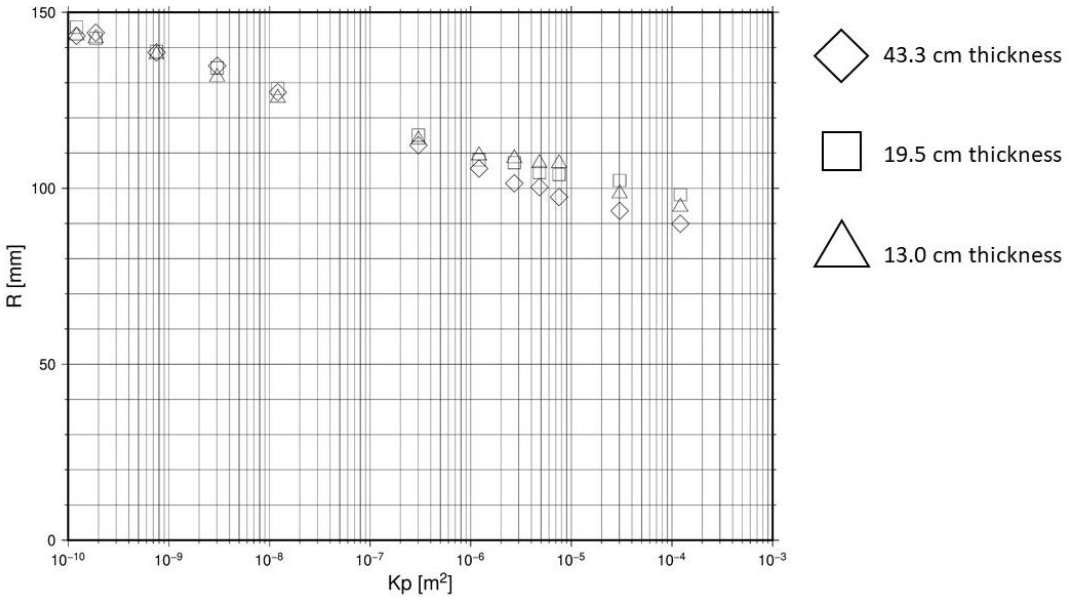

Figure 16. Runup height on 1:2.08 sloped porous layers with H = 0.0525 m

5.2 A 1:20 slope

This section simulates the wave runup on a mild slope covered with a porous layer of different thickness and permeability. The schematic of the computational domain is illustrated in Figure 17. The porous layer is placed with its bottom left corner at x = 2.0 m, and the beach slope is 1:20. The wave of height H = 0.0588 m is generated at the left end by the piston-type wavemaker. The porosity of the porous layers is fixed at 0.49, and the permeability ranges from 1.21×10^{-10}m^2 to 1.21×10^{-4}m^2. The thickness of the

porous layers varies from 7.5 cm, 20.0 cm, to 40.0 cm. The numerical parameters are listed in Table 4.

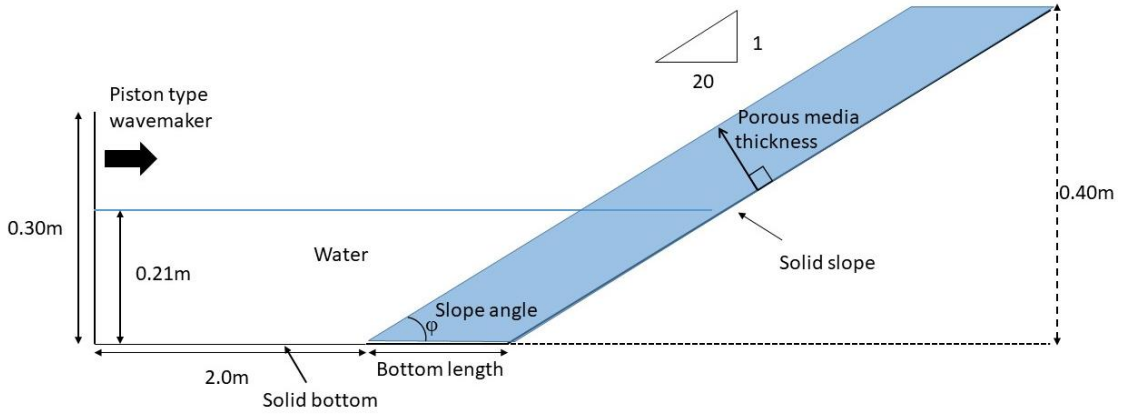

Figure 17. Setup of a 1:20 sloped porous layer

Table 4. Computational parameters for wave runup on 1:20 sloped porous layers

Parameters	Values
Diameter of particles (m)	0.005
Initial particle spacing of fluid particles (m)	0.005
Particle spacing of porous particles (m)	0.007
Smoothing length (m)	0.0085
Initial time step (s)	0.00025
Permeability of porous media (m^2)	1.21×10^{-10}, 1.88×10^{-10}, 7.54×10^{-10}, 3.02×10^{-9}, 1.21×10^{-9}, 3.02×10^{-7}, 1.21×10^{-6}, 2.71×10^{-6}, 4.82×10^{-6}, 7.54×10^{-6}, 3.02×10^{-5}, 1.21×10^{-4}
Bottom length of porous layers (cm)	150, 400, 800
Thickness of porous layers (cm)	7.5, 20.0, 40.0

Figure 18 captures the snapshots of solitary wave runup on a 7.5-cm-thick porous layer, with the permeability $Kp = 3.02\times 10^{-9}m^2$. The wave begins to break while running up the porous layer at t = 5.5 s, and is seen to reach the highest point at t = 8.60 s. Some

fluid particles plunged into the porous layer. Despite some small pressure disturbances observed at the toe of the slope, the overall obtained pressure field is smooth and rational.

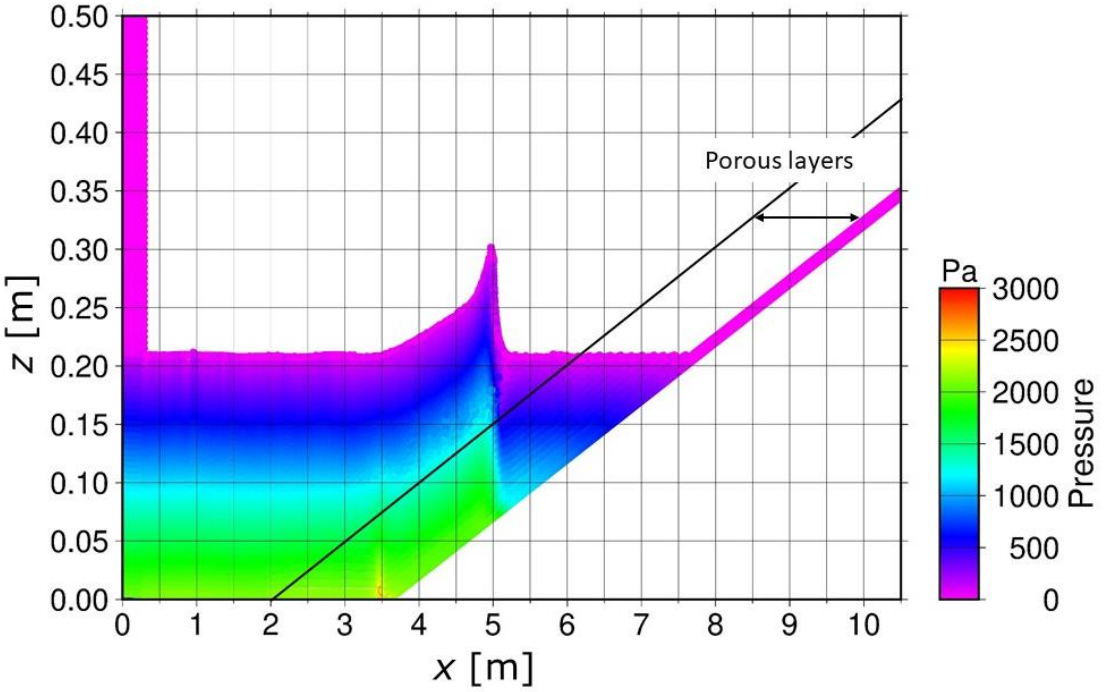

(a) t = 5.50 s

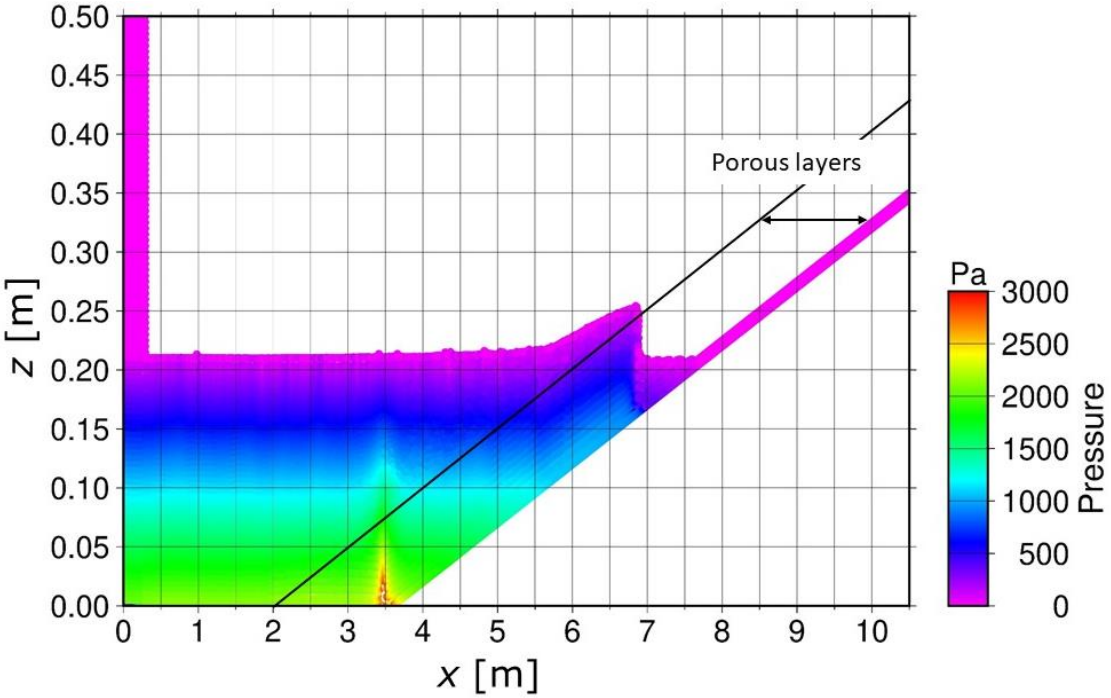

(b) t = 8.60 s

Figure 18 Wave runup on 7.5-cm-thick porous layers with $Kp = 3.02\times 10^{-9}$ m^2

Figure 19 compares the runup heights on the porous layers of different thickness and permeability. Similar to the results for nonbreaking waves, the runup height decreases with the increasing permeability. On this logarithmic graph, the relationship is nearly linear. The runup height is seen to be insensitive to the layer thickness, even when the permeability is very large. This result differs from the trend of nonbreaking waves as discussed in the previous section. On a mild slope, energy dissipates significantly when the wave breaks. Fluid particles can penetrate the porous boundary but cannot move over a long distance due to the weakened momentum after wave breaking, which yields almost the same runup height regardless of the layer thickness.

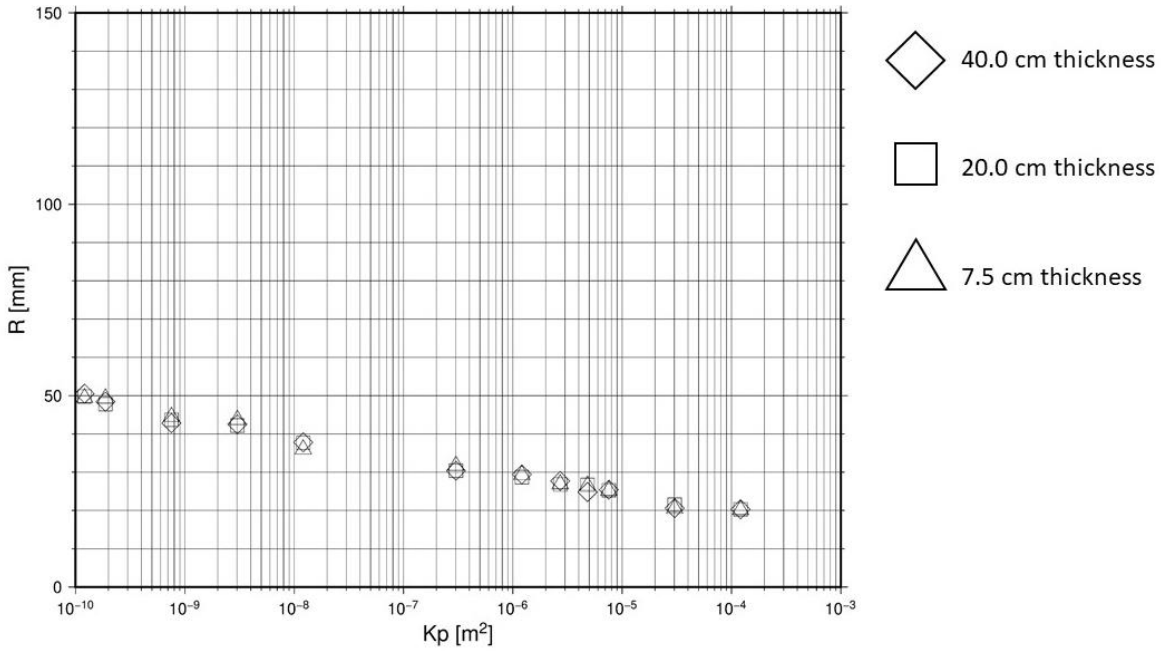

Figure 19. Runup height on a 1:20 sloped porous layers slope

A summary of the wave runup heights on triangular permeable beach and permeable layered beach is shown in Figure 20. It confirms that the runup height on such a mild

slope is insensitive to the thickness of the porous layer or the shape of the porous region. The wave breaking occurs on the mild slope, and the runup is seen to be the same as long as the permeability is the same, regardless of where the whole beach is permeable or the beach is just covered with a permeable layer. Consequently, the empirical equation (35), proposed for triangular permeable beaches, is also applicable to permeable layers overlying a solid slop.

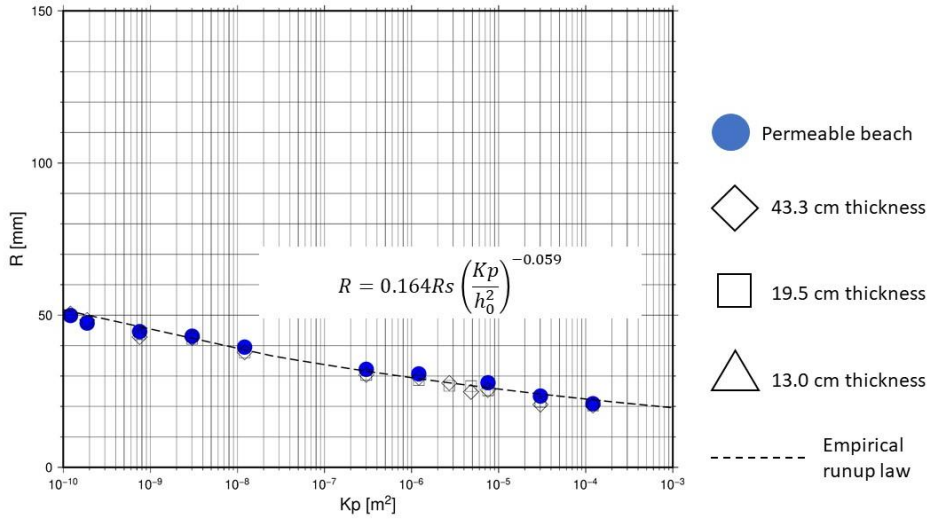

Figure 20 A summary of the wave runup on different types of 1:20 slopes (H/h_0 = 0.28)

6. Conclusions

Solitary wave runup on permeable beaches has been simulated using an ISPH model. In the present model, the location of the porous structure is described by porous particles which facilitate the determination of the apparent density and apparent volume of the fluid particle inside the porous structure. These apparent values take into account the fact that

fluid particles can only occupy the intergranular space. The current treatment guarantees the consistency of SPH interpolation.

After model verification against the runup on solid beaches, two different types of porous slopes have been extensively studied: one with the entire beach being porous and the other where the solid beach is covered by a porous layer. The runup height is found to decrease with the permeability according to a power law. Fluid particles cannot penetrate into a porous region if the permeability is sufficiently small. Empirical formulae have been proposed to predict the wave runup heights on porous beaches, using the runup heights on solid beaches as references. By substituting the solid slope runup equations of Synolakis (1986) into these empirical formulae, the direct relationships between the runup heights on permeable slopes and the water depth, wave height and slope angle can be derived. On beaches covered with a layer of porous medium, the runup height of nonbreaking waves is dependent on both the layer permeability and the thickness. Once the permeability exceeds a threshold value, then a thicker layer results in a lower runup height. For breaking waves, the runup height is not sensitive to the thickness of the porous layer and thus the permeability is the dominant influencing factor.

The present paper contributes to the insufficient numerical study of wave interaction with porous structures, but many issues demand further study. Because of the high computational cost, our parametric studies do not cover a large space. In the future, we will examine a broad range of parameters, including the beach slope, water depth, wave height and permeable layer thickness to further confirm the findings obtained in this study. It should be noted that the present study only focuses on the influence of permeability, while porosity is kept constant. It also assumes the smooth surface of the porous structure and the constant transition length between the pure fluid region and porous region. These

assumptions may not be applicable to many natural porous structures, as permeability, porosity, surface roughness and transition length are often altered simultaneously with the grain size or stem diameter. Further complications will arise when considering the heterogeneity of the porous structure, which may require the use of variable smoothing length. More advanced turbulence models (Wang and Liu, 2020) shall also be incorporated to improve the present results.

Acknowledgements

The research is supported by the National Natural Science Foundation of China (No. 51679036), Royal Society (No. IEC/NSFC/191369) and the Cambridge Tier-2 system operated by the University of Cambridge Research Computing Service (www.hpc.cam.ac.uk) funded by EPSRC Tier-2 capital grant EP/P020259/1. We are also thankful to Professor Songdong Shao from the University of Sheffield for sharing with us the original ISPH code and many valuable suggestions.

References

Akbari, H. (2014). Modified moving particle method for modeling wave interaction with multi layered porous structures. *Coastal engineering*, *89*, 1-19.

Akbari, H. & Torabbeigi M. (2021). SPH modeling of wave interaction with reshaped and non-reshaped berm breakwaters with permeable layers. *Applied Ocean Research*, 112, 102714.

Carrier, G. F., & Greenspan, H. P. (1958). Water waves of finite amplitude on a sloping beach. *Journal of Fluid Mechanics*, 4(1), 97-109.

Chang, Y. H., Hwang, K. S., & Hwung, H. H. (2009). Large-scale laboratory measurements of solitary wave inundation on a 1: 20 slope. *Coastal engineering*, 56(10), 1022-1034.

Goring, D. G. (1978). Tsunamis--the propagation of long waves onto a shelf. PhD thesis, California Institute of Technology.

Gotoh, H., Shibahara T. & Sakai, T. (2001). Sub-Particle-Scale Turbulence Model for the MPS Method – Lagrangian Flow Model for Hydraulic Engineering. *Computational Fluid of Dynamic Journal*, 9(4), 339–347.

Gotoh, H., Shao, S., & Memita, T. (2004). SPH-LES model for numerical investigation of wave interaction with partially immersed breakwater. *Coastal Engineering Journal*, *46*(01), 39-63.

Gui, Q., Dong, P., & Shao, S. (2015). Numerical study of PPE source term errors in the incompressible SPH models. *International Journal for Numerical Methods in Fluids*, *77*(6), 358-379.

Hall Jr, J. V., & Watts, G. M. (1953). *Laboratory investigation of the vertical rise of solitary waves on impermeable slopes*. Report No. TM33, ARMY COASTAL ENGINEERING RESEARCH CENTER, WASHINGTON DC, USA.

Hsiao, S. C., Hsu, T. W., Lin, T. C., & Chang, Y. H. (2008). On the evolution and run-up of breaking solitary waves on a mild sloping beach. *Coastal Engineering*, 55(12), 975-988.

Hughes, S. A. (2004). Estimation of wave run-up on smooth, impermeable slopes using the wave momentum flux parameter. *Coastal Engineering*, *51*(11-12), 1085-1104.

663 Katell, G., & Eric, B. (2002). Accuracy of solitary wave generation by a piston wave
664 maker. *Journal of Hydraulic Research*, *40*(3), 321-331.
665 Kazemi, E., Koll, K., Tait, S., & Shao, S. (2020). SPH modelling of turbulent open
666 channel flow over and within natural gravel beds with rough interfacial
667 boundaries. *Advances in Water Resources*, *140*, 103557.
668 Kazemi, E., Tait, S., & Shao, S. (2020). SPH- based numerical treatment of the interfacial
669 interaction of flow with porous media. *International Journal for Numerical*
670 *Methods in Fluids*, *92*(4), 219-245.
671 Khayyer, A., Gotoh, H., & Shao, S. (2009). Enhanced predictions of wave impact pressure
672 by improved incompressible SPH methods. *Applied Ocean Research*, *31*(2), 111-
673 131.
674 Khayyer, A., Gotoh, H. & Shimizu, Y. (2017). Comparative study on accuracy and
675 conservation properties of two particle regularization schemes and proposal of
676 an optimized particle shifting scheme in ISPH context. *Journal of*
677 *Computational Physics*, 332, 236–256.
678 Khayyer, A., Gotoh, H., Shimizu, Y., Gotoh, K., Falahaty, H., & Shao, S. (2018).
679 Development of a projection-based SPH method for numerical wave flume with
680 porous media of variable porosity. *Coastal Engineering*, 140, 1-22.
681 Kim, N. H., & Ko, H. S. (2008). Numerical simulation on solitary wave propagation and
682 run-up by SPH method. *KSCE Journal of Civil Engineering*, *12*(4), 221-226.
683 Li, Y., & Raichlen, F. (2001). Solitary wave runup on plane slopes. *Journal of Waterway,*
684 *Port, Coastal, and Ocean Engineering*, 127(1), 33-44.
685 Liang, D., Gotoh, H., Khayyer, A., & Chen, J.M. (2013a). Boussinesq modelling of
686 solitary wave and N-wave runup on coast. *Applied Ocean Research*, 42: 144-154

687 Liang, D., He, X., Zhang, & J. (2017). An ISPH model for flow-like landslides and
688 interaction with structures. *Journal of Hydrodynamics*, 29(5), 894-897
689 Liang, D., Liu, H., Tang, H., & Rana, R. (2013b). Comparison between Boussinesq and
690 shallow-water models in predicting solitary wave runup on plane beaches,
691 *Coastal engineering journal*, 55(4), Article No 1350014
692 Lin, P., Chang, K. A., & Liu, P. L. F. (1999). Runup and rundown of solitary waves on
693 sloping beaches. *Journal of waterway, port, coastal, and ocean engineering*,
694 125(5), 247-255.
695 Lind, S.J., Xu R., Stansby, P.K. & Rogers, B.D. (2012). Incompressible smoothed particle
696 hydrodynamics for free-surface flows: A generalised diffusion-based algorithm
697 for stability and validations for impulsive flows and propagating waves. *Journal*
698 *of Computational Physics*, 231, 1499–1523.
699 Liu, P. L. F., Lin, P., Chang, K. A., & Sakakiyama, T. (1999). Numerical modeling of
700 wave interaction with porous structures. *Journal of waterway, port, coastal, and*
701 *ocean engineering*, *125*(6), 322-330.
702 Lo, E. Y., & Shao, S. (2002). Simulation of near-shore solitary wave mechanics by an
703 incompressible SPH method. *Applied Ocean Research*, *24*(5), 275-286.
704 Harris, L., Liang, D., Shao, S., Zhang, T., & Roberts, G. (2021). MPM Simulation of
705 Solitary Wave Run-up on Permeable Boundaries. *Applied Ocean Research*, 111,
706 Article No 102602.
707 Memarzadeh, R., & Hejazi, K. (2012). ISPH numerical modeling of nonlinear wave run-
708 up on steep slopes. *Journal of the Persian Gulf, 3(10),* 17-26.
709 Monaghan, J. J., & Kos, A. (1999). Solitary waves on a Cretan beach. *Journal of*
710 *waterway, port, coastal, and ocean engineering*, *125*(3), 145-155.

711 Pahar, G., & Dhar, A. (2017). Numerical modelling of free-surface flow-porous media
712 interaction using divergence-free moving particle semi-implicit method.
713 *Transport in Porous Media*, *118*(2), 157-175.
714 Peng, C., Xu, G., Wu, W., Yu, H. S., & Wang, C. (2017). Multiphase SPH modeling of
715 free surface flow in porous media with variable porosity. *Computers and*
716 *Geotechnics*, *81*, 239-248.
717 Qu, K., Sun, W. Y., Deng, B., Kraatz, S., Jiang, C. B., Chen, J., & Wu, Z. Y. (2019).
718 Numerical investigation of breaking solitary wave runup on permeable sloped
719 beach using a nonhydrostatic model. *Ocean Engineering*, *194*, 106625.
720 Ren, B., Wen, H., Dong, P., & Wang, Y. (2016). Improved SPH simulation of wave
721 motions and turbulent flows through porous media. *Coastal Engineering*, *107*,
722 14-27.
723 Shadloo, M. S., Weiss, R., Yildiz, M., & Dalrymple, R. A. (2015). Numerical simulation
724 of long wave runup for breaking and nonbreaking waves. *International Journal*
725 *of Offshore and Polar Engineering*, *25*(01), 1-7.
726 Shao, S. (2010). Incompressible SPH flow model for wave interactions with porous media.
727 *Coastal Engineering*, *57*(3), 304-316.
728 Shao, S., Lo, E. Y. M. (2003). Incompressible SPH method for simulating Newtonian and
729 non-Newtonian flows with a free surface. Advances in water resources, 26(7),
730 787-800.
731 Synolakis, C. E. (1986). *The runup of long waves.* PhD thesis, California Institute of
732 Technology.
733 Synolakis, C. E. (1987). The runup of solitary waves. *Journal of Fluid Mechanics*, *185*,
734 523-545.

Tsurudome, C. (2020). ISPH Modelling of Solitary Wave Interaction with Permeable Beaches. PhD thesis, University of Cambridge. https://www.repository.cam.ac.uk/handle/1810/308413

Tsurudome, C., Liang, D., Shimizu, Y., Khayyer, A., & Gotoh, H. (2020). Incompressible SPH simulation of solitary wave propagation on permeable beaches. *Journal of Hydrodynamics*, *32*(4), 664-671.

Wang, D., & Liu, P. L. F. (2020). An ISPH with k–ε closure for simulating turbulence under solitary waves. *Coastal Engineering*, *157*, 103657.

Wen, H., Ren, B., Dong, P., & Zhu, G. (2020). Numerical analysis of wave-induced current within the inhomogeneous coral reef using a refined SPH model. *Coastal Engineering*, *156*, 103616.

Wendland, H. (1995). Piecewise polynomial, positive definite and compactly supported radial functions of minimal degree. *Advances in Computational Mathematics*, 4, 389-396.

Xiao, H., & Huang, W. (2008). Numerical modeling of wave runup and forces on an idealized beachfront house. *Ocean Engineering*, *35*(1), 106-116.